Expansion of a multi-component laser-ablated plume

A.M. Slowicka, Z.A. Walenta, Z. Szymanski

Expansion of a multi-component laser-ablated plume

A M Slowicka, Z A Walenta and Z Szymanski

Institute of Fundamental Technological Research, Pawinskiego 5B,
02-106 Warsaw, Poland

Email: aslowick@ippt.gov.pl

Abstract. The expansion of a plume generated during laser ablation is studied with the Direct Simulation Monte Carlo method. The plume is a mixture of four disparate molecular mass components and expands in vacuum or into ambient gas. The time dependence of deposition rate is studied and the transition from an initial vacuum-like to a diffusion-like regime of expansion in ambient gas is shown. The lack of stoichiometry increases with the ratio of molecular masses of ablated particles and at disparate masses the stoichiometry is seriously affected. Ambient gas worsens the stoichiometry unless it supplies particles compensating the backward and sideward flows of plume constituents.

Keywords: laser ablation, pulsed laser deposition, DSMC, hydroxyapatite
PACS: 52.38.Mf, 02.60.Cb

1. Introduction

Pulsed laser deposition (PLD) is a powerful method for obtaining thin films. One of the usually mentioned advantages of this method is, that stoichiometry is preserved. This should result from the fact that high energy flux to the surface of a target causes all material constituents to be vaporized practically at the same time, regardless of their evaporation temperature. The stoichiometry is, in fact, preserved only in the vicinity of a target. At further distances it is lost due to differences in molecular masses of the expanding elements and resulting differences in the rates of their expansion. Therefore one of the problems that needs a better understanding is the expansion of the evaporated material in vacuum or into a background gas. The direct simulation Monte Carlo (DSMC) method seems to be a proper tool for studying the expansion of the ablated plume after its initial high pressure expansion because the standard gasdynamical description becomes very complex in the case of many

components. The expansion of ablated particles was studied with the use of the Monte Carlo method by several authors [1-8]. In particular the problem of stoichiometry was studied in [1,2,8].

In [1] the ablation of a binary target in vacuum was studied. The mass ratio of ablated particles was M_1:M_2 = 1:5. In [2] the mass ratio of ablated particles was M_1:M_2 = 1:2 and the mass ratio of ambient gas particles to lighter particles M_3:M_1 was 0.63. The test particle method was applied i.e., collisions between plume molecules and the post-collision motion of the background gas molecules were neglected. In both papers [1,2] the mean thermal velocity of ablated particles corresponding to the surface temperature was assumed as an initial condition. In both papers a deficiency of light particles close to the substrate centre was found. It was also found that lighter particles move faster, which results from the assumption that all species desorb from the target with the mean thermal velocity corresponding to the same temperature.

In PLD multicomponent targets often contain elements with disparate masses. Such a situation is present in the case of the hydroxyapatite target ($Ca_{10}(PO_4)_6(OH)_2$), YBCO target or super hard materials like LaB_6 or ReB_2. In the present paper the expansion of a plasma plume, consisting of four kinds of particles with disparate molecular masses M_1= 40, M_2 = 31, M_3 = 16, M_4 = 1, is studied with the Direct Simulation Monte Carlo method. The ablation takes place in vacuum or in an ambient gas with M_5 = 18, so the mass ratio of the plume constituents to the background gas is in the range from 2.2 to 0.055. In contrast to [1,2], according to experimental evidence, the shifted Maxwellian distribution of ablated particles, which includes a directed macroscopic velocity, has been assumed as an initial condition. The DSMC method is applied so both collisions between plume molecules and the post-collision motion of the background gas molecules are taken into account.

The considered process is related to the pulsed laser deposition of hydroxyapatite ($Ca_{10}(PO_4)_6(OH)_2$), where the mass of hydrogen is very much different from the masses of other particles. Synthetic hydroxyapatite (HA) is a biocompatible ceramic. It is chemically similar to the mineral component of mammalian bone. For this reason, the human body (and bodies of other mammals as well) can assimilate HA. HA is deposited onto orthopaedic implants in order to improve the bone-implant contact. Good quality HA coatings are obtained when the ambient gas is water vapour at a pressure of 10-150 Pa [9-12]. Comprehensive literature can be found in [13]. A theoretical study of the expansion of species ablated during pulsed laser deposition of hydroxyapatite is undertaken for a better understanding of this problem.

2. Model of the plume expansion

During the first 100-200 nanoseconds after the beginning of the laser pulse, the plume is so dense that it can be treated as a continuum fluid and equations of gasdynamics can be applied for its description. A continuous modelling is usually applied for time $t = 10\ \tau$, where τ is the pulse width [4,5]. As initial conditions the conditions at the end of the Knudsen layer are assumed [14,15]. Later, when ionization processes are not significant, the Direct Monte Carlo Simulation method may be used successfully [4,5].

In our calculations we assumed that time t_0 corresponds to time ~300 nanoseconds after the laser pulse. At that time the particles have the Maxwellian distribution with a temperature of 6000 K, and a macroscopic mass centre velocity normal to the surface, $v_0 = 1\times10^4$ m·s^{-1}. Both values are based on experimental results of the HA ablation [16]. However, the temperature assumed is much lower as compared to the value of 10500 K found in [16] for that moment. The temperature was diminished deliberately because the results reported in [16] were obtained at a rather high laser fluence F = 7 J·cm^{-2}, while HA films are usually deposited at a 2-3 times lower fluence. The degree of ionization was estimated as ~ 0.014 (about half of calcium atoms is ionized, while other species are not). The estimation was made by solving a system of coupled Saha equations for the mixture of species that constitute hydroxyapatite at conditions corresponding to the initial moment of the calculations (p ~ 15 kPa). After 100 ns, the temperature drops to 5000 K and the ionization degree to 0.05. These estimations justify to a degree the simplified model of collisions applied in this paper.

We assumed that at time t_0 the plume is spherical with a radius of 2.5 mm and the total number of plume particles is 1×10^{16} . The estimation of the total number of particles desorbed from the target in a single laser pulse is based on [17], assuming the focal spot about 1mm^2. The plume centre is located 3 mm from the target surface.

Collisions with ions were not taken into account. The degree of ionization at a temperature of 6000 K is small. The transfer of momentum between atoms and electrons is negligible due to the small mass of the electron. At later times, ionization degree decreases due to recombination processes, and collisions with ions become even less important. However, a thermal dissociation of the water vapour molecules, which may be essential for the considered process, was taken into account. The cross section for collisions between neutral particles is given by the Variable Hard Sphere model [18] in which the diameter of a molecule is $\sigma = \sigma_{ref}\ (v_{ref}/v)^i$, v is the relative velocity of the colliding particles, i is a parameter determined by the viscosity temperature power law and subscript *ref* denotes the reference value. The atomic

diameters σ_{ref} (at T_{ref} =300 K) for H, O, Ca, and P atoms were taken respectively as 0.281 nm [19], 0.295 nm [19], 0.4 nm [20] and 0.36 nm [20]. σ_{ref} = 0.31 [21] was assumed for water vapour molecules. i = 0.3 was assumed for all atomic gases. Such values were derived from the viscosity of atomic oxygen [22] and hydrogen [23]. Since the temperature dependence of the viscosity is not available for Ca and P, the same values of i = 0.3 were assumed. For water vapour i = 0.6 was adopted [24]. The ballot-box scheme for the selection of colliding pairs that allows the use of a small number of model particles was employed [25].

The initial calculation domain was cylindrical, 13 mm high, and with a radius of 9 mm. The final domain was 40 mm high and with a radius of 27.5 mm. The lower wall represented the shield of a target holder, the upper wall (h = 40 mm) - a substrate. The whole domain was split into cells of an equal volume. Calculations were performed for the expansion into vacuum and the ambient atmosphere of the water vapour at an initial pressure of 20 Pa and a temperature of 300 K. The initial mean free path λ for collisions between plume particles was ~ 0.04 mm, and this value and the time between collisions $\tau \approx 0.35$ ns determined the initial cell dimension and the computational time step. The initial Knudsen number defined as $Kn=\lambda/D$ where λ is the mean free path and D is the diameter of the plume was 0.008.

The cell dimension and the time step were kept no bigger than $\lambda/2$ and $\tau/10$ throughout the calculations, except for the first few hundred nanoseconds when the cell dimension was only smaller than λ. The initial numbers of particles representing the plume and the water vapour were about 6.3 and 9.7 million, respectively; one "representative particle" corresponded to about 4×10^8 real molecules. During the expansion of the plume the simulated domain was gradually increased and the volume of the cell was increased too. As already mentioned, the final domain was 40 mm high with a radius of 27.5 mm. It means that the volume of the calculation domain increased ~ 29 times. The water vapour was distributed uniformly so the number of particles representing it should be increased 29 times, which was over the capacity of the computer. Instead the number of real molecules represented by one "representative particle" was increased 29 times, to about 1.16×10^{10}. As a result the number of particles representing the water vapour remained unchanged and the number of particles representing the plume had to be decreased about 29 times, down to 0.217 million.

The plume particles disappeared from the calculation domain when they hit boundaries except for the hot focal spot of the laser beam where a diffuse reflection [18] took place.

The dissociation of water vapour molecules was considered as a two step process: at first – the dissociation of a H_2O molecule into an OH hydroxyl radical and an H atom, next – the dissociation of the hydroxyl radical OH into H and O atoms. The equipartition of energy between all resulting particles after the dissociating collision was assumed. The values of dissociation energies (5.1 eV and 4.4 eV, respectively) were taken from [26]. It was assumed that the dissociation took place during a collision of two molecules if the translational energy along the line between their centres exceeded the corresponding dissociation energy [18]. The typical procedures based on equilibrium models like the Larsen-Borgnakke distribution or fitting to the known reaction rates are rather useless in this case. The water vapour in front of the plume is in the state of equilibrium and the presence of the internal degrees of freedom has little influence upon the net result of collisions. The dissociation takes place due to collisions of energetic plume particles (a velocity of 1×10^4 m·s^{-1} corresponds to an energy of 21 eV in the case of Ca atoms and 8 eV in the case of O atoms) with practically motionless water vapour molecules. Collisions of such energetic molecules lead, within the framework of the assumed model, to an immediate dissociation of H_2O without a gradual excitation of internal degrees of freedom.

3. Results and discussion

3.1. Expansion into vacuum

Contour maps of number densities of two plume components: calcium (Ca) and hydrogen (H) in the case of ablation in vacuum at time t =1900 ns after the beginning of the calculation are presented in Fig.1. Oxygen and phosphorus are not shown because their density contours are similar to those of calcium. Different sizes of clouds of calcium and hydrogen result from a faster expansion (relative to the mass centre) of lighter particles at a given temperature. Calcium and phosphorus particles come together because their molecular masses are relatively close to each other and stoichiometry is preserved in this case. The clouds of molecules are spherically symmetric, which results from the assumed velocity distribution. The velocities of the plume front obtained from the present calculations are about 2×10^4 m·s^{-1} and are similar to those observed in experiments [16, 27].

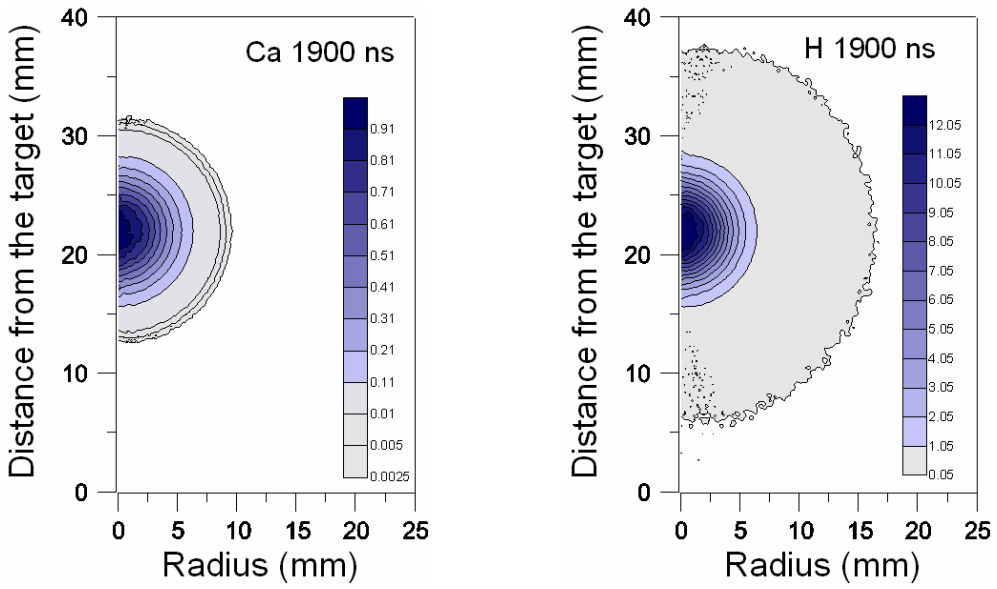

Fig.1. Contours of number densities of plume components ($N \times 4.9 \times 10^{15}$ cm^{-3}) at t = 1900 ns. Expansion in vacuum.

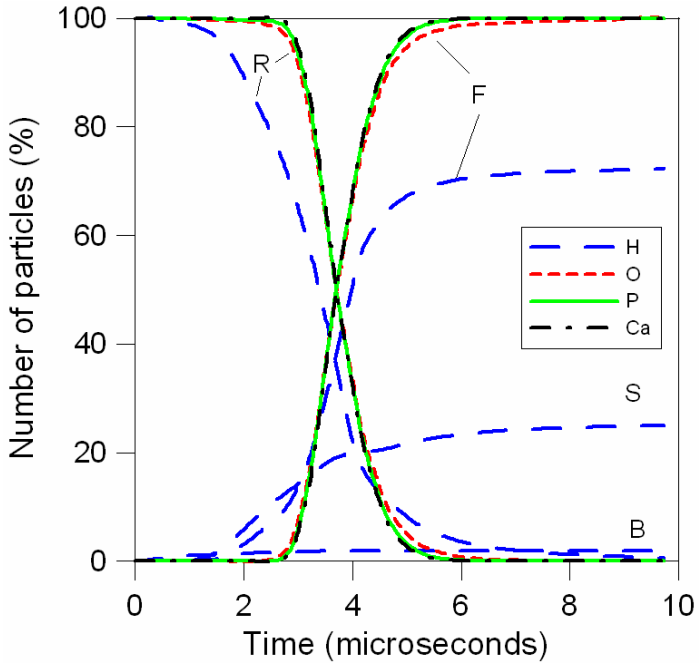

Fig.2. Location of particles (related to the total number of particles of a given kind) as a function of time; *F* – particles deposited at the substrate, *B* and *S* – particles which have left the domain through the back and side boundaries correspondingly, *R* – remainder. Expansion in vacuum.

Figure 2 shows the location of particles (related to the total number of particles of a given kind) as a function of time. The deposition process is terminated after 10 μs. It is evident from the presented results that all Ca, P and O particles reach the substrate during that

time (and are deposited assuming a sticking coefficient equal unity). In contrast to heavier particles, the amount of hydrogen that reaches the substrate is only ~72.5 % of the total number of hydrogen atoms. The number of H atoms leaving the domain through the side boundary is significant and it amounts to 25 % of total. About 2% have moved backward and are deposited on the target holder while ~0.5 % still remain in the calculation domain.

The presented maps show that the stoichiometry cannot be preserved when ablating hydroxyapatite in vacuum. A large amount of hydrogen is lost through the side boundary and some on the target holder. Some hydrogen atoms move backward because their thermal speed 1.12×10^{4} m·s^{-1} exceeds their macroscopic forward velocity 1×10^{4} m·s^{-1}. The resulting deficit of hydrogen is mainly responsible for the lack of the desired stoichiometry in films deposited in vacuum.

Fig. 3 presents normalized spatial distributions of the number of particles per unit area deposited on the substrate as a function of a radial distance from the centre of the substrate. The normalization is made as follows. First, the number of the deposited Ca atoms is normalized to their maximum at the centre. Afterwards densities of other particles are normalized to their stoichiometric values with respect to the density of deposited Ca atoms. This means that, for example, at the substrate centre the amount of deposited H atoms is only ~ 45 % of their stoichiometric value.

The results are compared with the density profiles resulting from the analytical fluid model of Anisimov [28]. In the case of heavy plume components the agreement is rather poor. This discrepancy results most probably from the fact that in Anisimov's model the initial gas cloud created near the target surface remains elliptical during its expansion. The characteristics of the expanding plasma plume are constant at ellipsoidal surfaces. The centre of these ellipsoids remains fixed at the target surface. In our calculations it has been assumed that the centre of the plume moves with a velocity of 1×10^{4} m·s^{-1} directed perpendicularly to the target. This velocity is dominant in the case of heavy particles. In the case of hydrogen, the directed velocity is smaller than the thermal velocity and hence the agreement between our results and the Anisimov theory is quite good. It is worth noting that in [29] it was found that the expansion of a laser-induced silver plume was in a fair agreement with the Anisimov theory. Perhaps the directed forward velocity was smaller in that case.

The presented distributions show an inhomogeneity of the deposited material. In the case of lighter particles the distribution is flatter. This again results from higher thermal velocity of lighter particles. The stoichiometric ratio of O:Ca/P is too low for the radii lower than 10 mm and it exceeds the target value for greater radii. The stoichiometric ratio of H:O is too low for the radius lower than 14 mm. The migration of the adsorbed atoms can reduce unhomogeneity of deposited material but the deficit of hydrogen will remain. However, post-deposition annealing in the air, which always contains some water vapour, restores the HA stoichiometry and results in crystalline hydroxyapatite coatings [30,31].

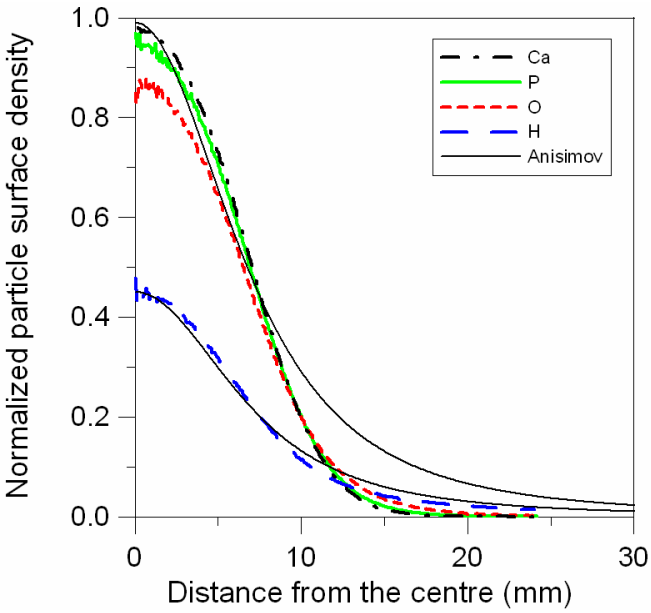

Fig.3. The normalized number of deposited particles per unit area as a function of radial distance from the centre of the substrate. Expansion in vacuum.

3.2. Expansion in the ambient gas

Contour maps of number densities of plume components (Ca and H) and the surrounding gas, in the case of ablation into the atmosphere of water vapour at a pressure of 20 Pa, at a time t=1900 ns are shown in Fig.4. Now the collisions with the surrounding H_2O molecules prevent hydrogen from a fast escape forward and to the sides. However, these collisions result in an increased backflow of hydrogen atoms to the target holder.

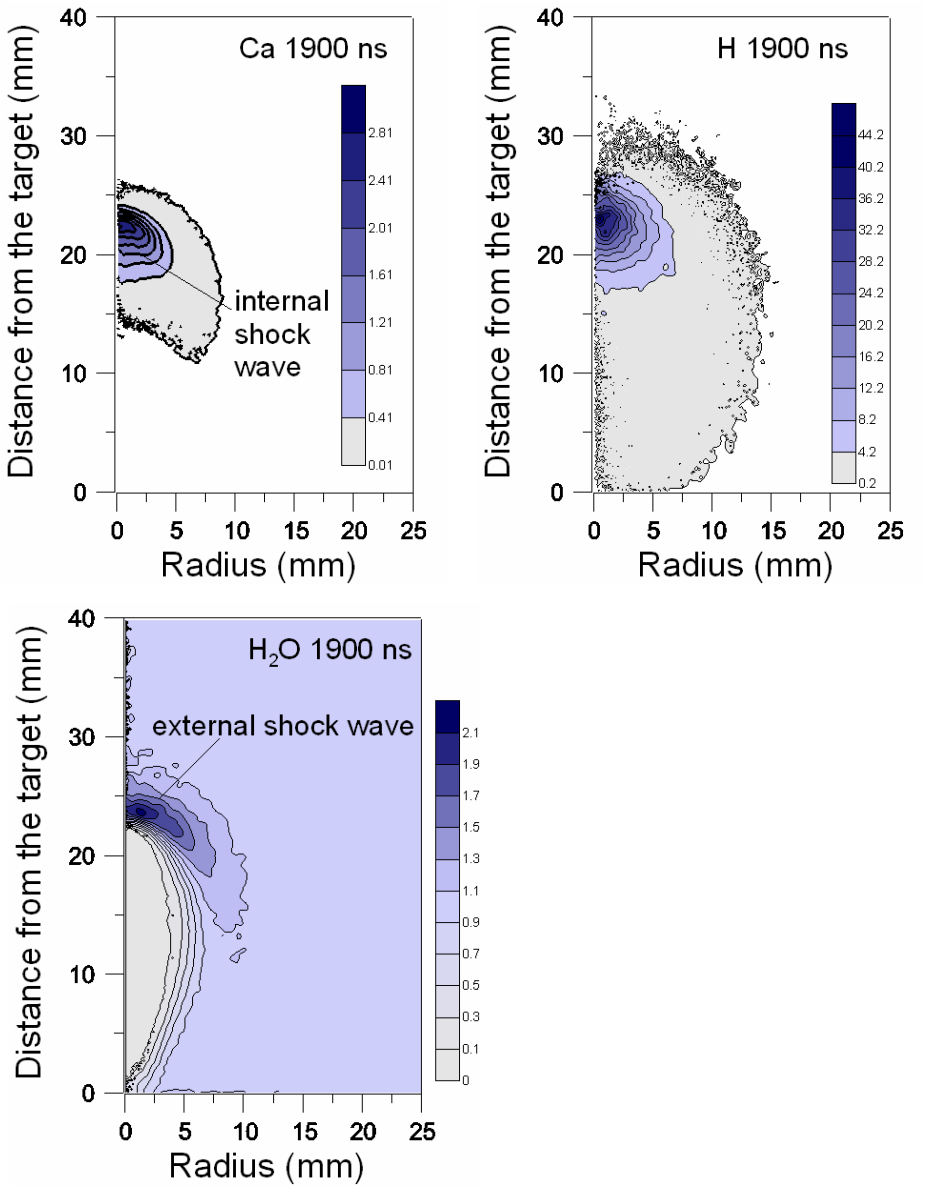

Fig.4. Number densities ($N \times 4.9 \times 10^{15}$ cm^{-3}) of the plume and ambient gas components at t = 1900 ns. Expansion into water vapour at a pressure of 20 Pa.

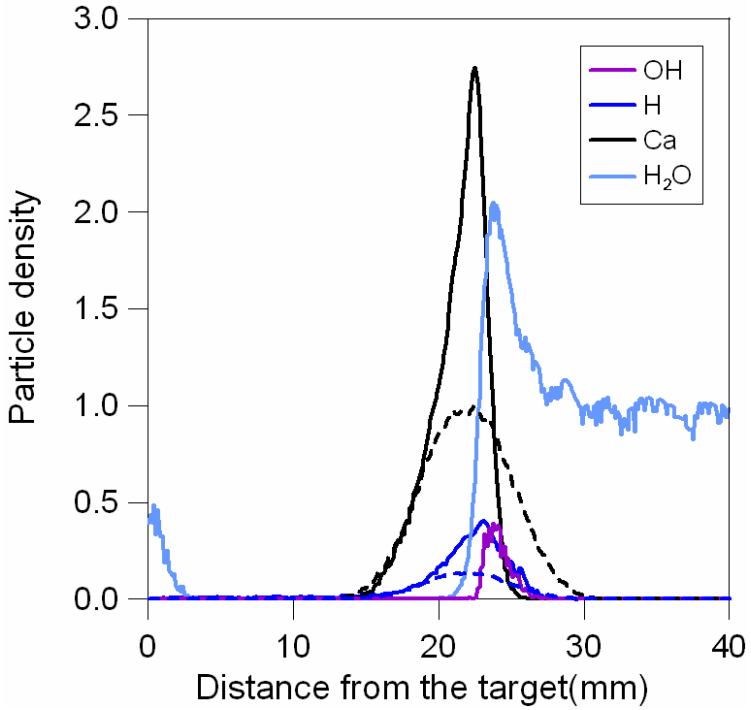

Fig.5. Profiles of the particle density ($N\times4.9\times10^{15}$ cm^{-3}) at the plume axis as a function of distance from the target. Solid line – water vapour, dashed line – vacuum.

The plume moves across the ambient gas like a snow plough, generating a bow shock wave in front of it. This shock is strong enough in its central part to heat the ambient gas – water vapour – to a temperature sufficient for its dissociation. As a result, an extra amount of hydrogen together with the hydroxyl radical (OH) appears in front of the plume (within the contour 1.1 of H_2O). Next the dissociation of OH takes place. It can be seen in Fig.5 where the profiles of the particle density at the plume axis are shown. The increased amount of hydrogen in comparison to the case of vacuum is clearly seen.

The velocities of the plume front obtained from the present calculations and experiments [16,32,33] are compared in Fig.6, where positions of the plume front in terms of time elapsed from the laser pulse are shown. In the case of expansion in water vapour the agreement between various experiments is poor. Our calculations are in a fair agreement with the results of Serra and Morenza with Nd:YAG laser at a wavelength of 355 nm, and a fluence F=1.5 J·cm^2 [32]. However, the most surprising is the lack of a correlation between various experiments. The front velocity in the case of KrF laser (243 nm) at a fluence of F=2.6 J·cm^2 [33] and a pressure of water vapour p = 10 Pa is lower and the velocity in the case of ArF laser (193 nm) at a fluence of F=7 J·cm^2 and an ambient pressure of 20 Pa [16] is even lower. According to the simple point blast model [34,35], the expansion of the plume into ambient

gas can be described by $R = \xi_0 \cdot \left(\frac{E}{\rho_0} \right)^{1/5} t^{2/5}$ where *R(t)* is the position of the shock wave front, E - is the energy of the detonation, ρ_0 – is the density of the ambient gas, t - is time, and ξ_0 is the coefficient close to unity. The energy of the laser pulse was 300 mJ in the case of ArF laser [16]. Although in other papers [32,33] the energy of the laser pulse was not mentioned the type of lasers used suggested that it should not be much different. In addition, the dependence both on the energy and the pressure in the above quoted formula is weak. In view of the discrepancies in experimental results any validation of our results is difficult.

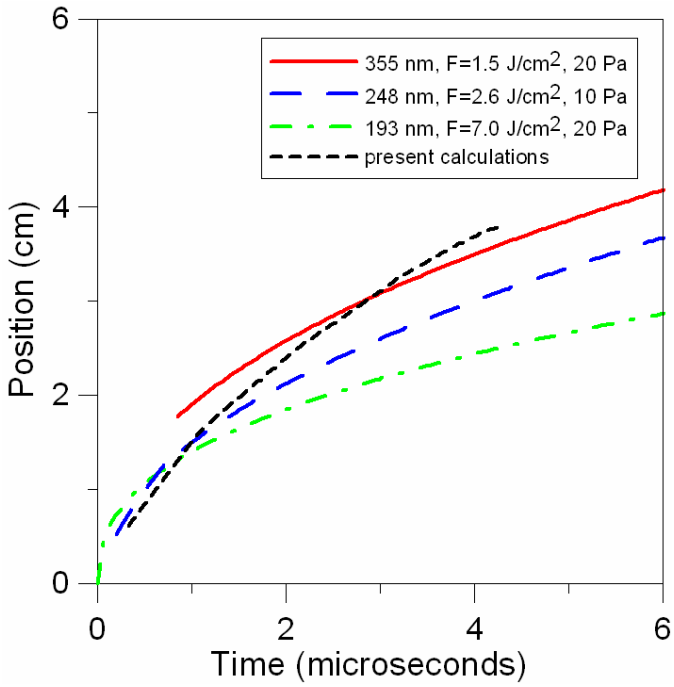

Fig.6. Position of the plume front vs. time after the laser pulse. Ambient gas is water vapour at pressures of 10 and 20 Pa.

Figure 7 shows the location of particles as a function of time. In the presence of an ambient gas, the plume particles are scattered in collisions with ambient gas molecules [7]. The results presented in Fig.7 and Fig.2 show how the ambient gas changes the deposition rate. The rapid vacuum-like expansion occurs up to t = 7 μs. After 7 μs the transition from the vacuum-like expansion to the diffusion-like regime takes place. At this time most of the plume observed in Fig. 4 already has passed the perimeter of h=40 mm, which means that it has been deposited on the substrate. However, part of the plume with much smaller density but occupying a much bigger volume is still in the calculation domain as a result of scattering.

This part of plume has a much smaller directed velocity and is slowly moving to the substrate. After 10 μs the expansion is governed mainly by diffusion. From this time on the backward and sideward movement of particles becomes significant. The lighter particles diffuse faster because the diffusion coefficient *D* scales as $M^{-1.4}$ [8].

After 70 μs the number of deposited Ca particles (M=40) is 54.9 % of the total number of particles of this kind, 8.3 % is scattered on sides, 0.1 % is backscattered and 36.7 % still remain in the calculation domain. In the case of P particles (M=31) the number of deposited particles is 47.5 %, 8.9 % is scattered on sides, 0.3 % is backscattered and 43.3 % still remain in the calculation domain. In the case of O atoms (M=16) the corresponding quantities are 40.6, 14.9, 2.2 and 45.7 %, respectively. The total amount of oxygen increases by 3 % due to the dissociation of OH radicals. It is worth noting that the stoichiometry is generally worse than in the case of the expansion in vacuum unless the particles supplied in the dissociation process compensate the back- and side-scattering effects. The loss of stoichiometry because of stronger scattering of lighter particles starts from the beginning and is already clearly seen after 4 μs when the first particles arrive at the substrate (see the inset). The number of hydrogen particles (M=1) that reach the substrate after 70 μs amounts to 96.6 % of the total number of emitted hydrogen atoms; 111 % is scattered on sides, 61 % is backscattered and 43.4 % still remain in the calculation domain. These results show that this time hydrogen is in excess as a result of the dissociation of the water vapour. The number of produced H atoms and OH radicals amounts to 9.6 and 7.4 % of the total number of ablated particles (10^{16}), respectively. For comparison the number of ablated hydrogen atoms is 4.5 %. The maximum of dissociation products is reached after about 3000 ns; after that time the kinetic energy of plume particles is too low to dissociate H_2O and OH molecules.

The stoichiometry of O:Ca:P:H elements in the HA target is 13:5:3:1. After 70 μs of the deposition in the ambient water vapour at a pressure of 20 Pa the stoichiometry of deposited O:Ca:P:H atoms is 13:6.1:3.2:3.5 including atoms in OH radicals. It means that there is a deficit of oxygen now, although oxygen from OH radicals makes 11.9 % of deposited oxygen atoms. In contrast to the deposition in vacuum the hydrogen is in excess now.

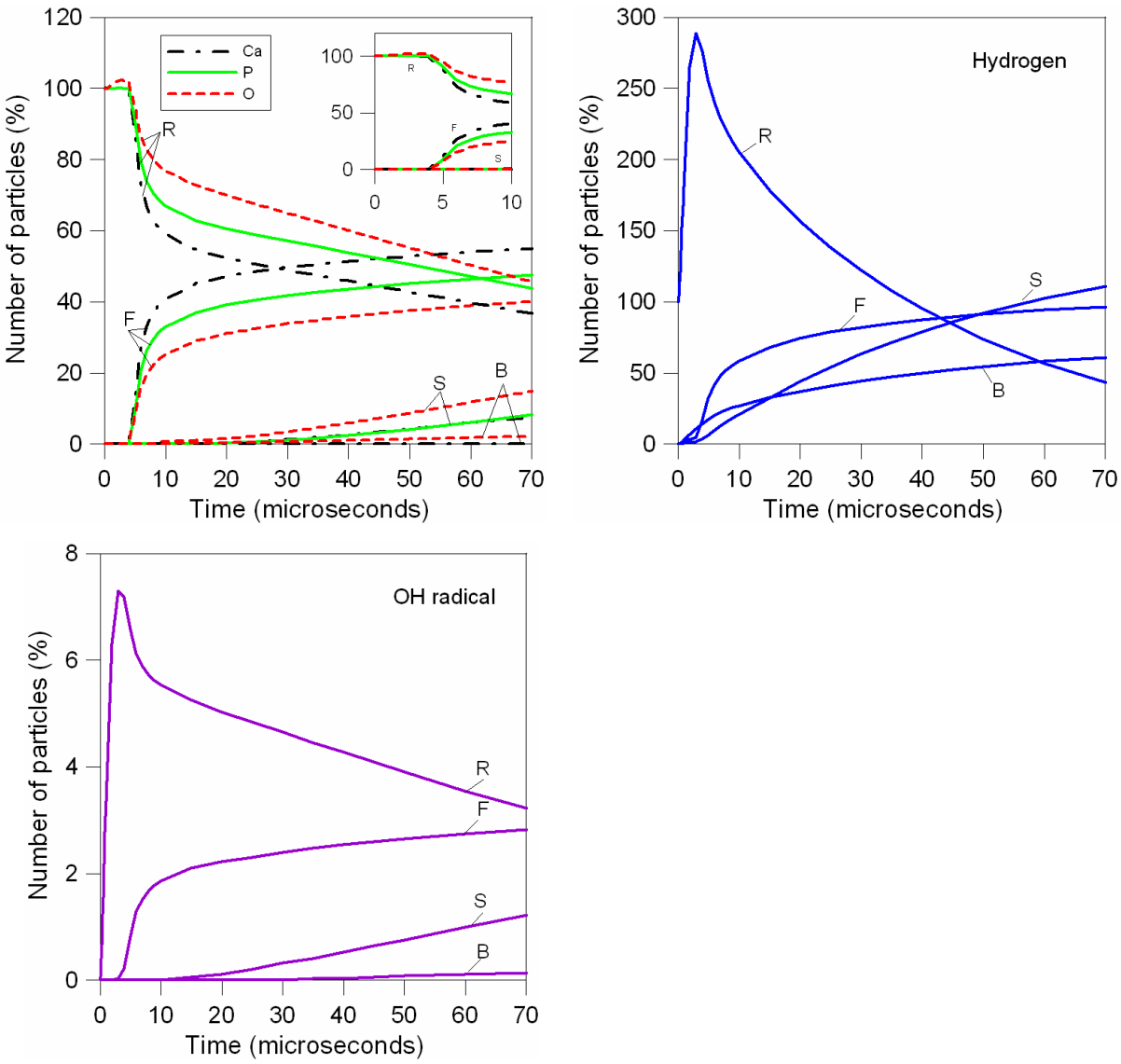

Fig.7. Location of particles (related to the total number of particles of a given kind)as a function of time; *F* – particles deposited at the substrate, *B* and *S* – particles which have left the domain through the back and side boundaries correspondingly, *R* – remainder. Expansion into water vapour at a pressure of 20 Pa. The number of OH radicals is related to the total number of ablated particles. The inset shows first 10 microseconds.

As mentioned before, contrary to the expansion in vacuum where the deposition process is completed after 10 μs, in the case of the expansion into water vapour the process is not completed even after 70 μs. However, after about 10 μs the character of deposition changes significantly. The decrease of the deposition rate is clearly seen in Fig.7, especially for the heaviest particles. As seen in Fig.8 the mean axial velocity of the ablated particles decreases to zero also in about 10 μs. From this time on, the deposition process is governed mainly by the diffusion. All kinds of particles reach each boundary of the calculation domain with the same probability. The significant backward and sideward movement starts after 10

μs. After 70 μs the spatial distribution of the particles that remain in the calculation domain is roughly homogeneous. A simple geometrical estimation shows that then no more than 20 % of remaining particles can reach the substrate. In a real experiment part of remaining particles will be removed from the chamber by a pumping system**.** Therefore after 70 μs the stoichiometry will not change significantly during a further expansion.

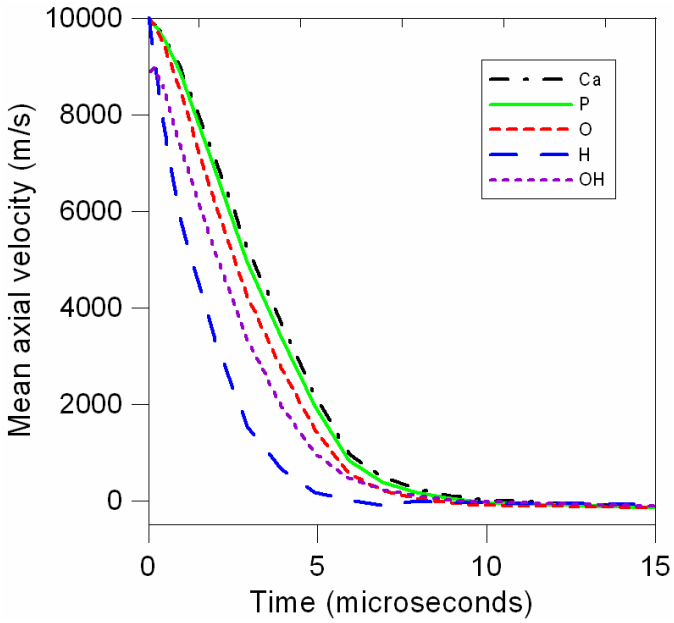

Fig.8. Mean axial velocities of ablated particles as a function of time. Ambient gas water vapour at a pressure of 20 Pa.

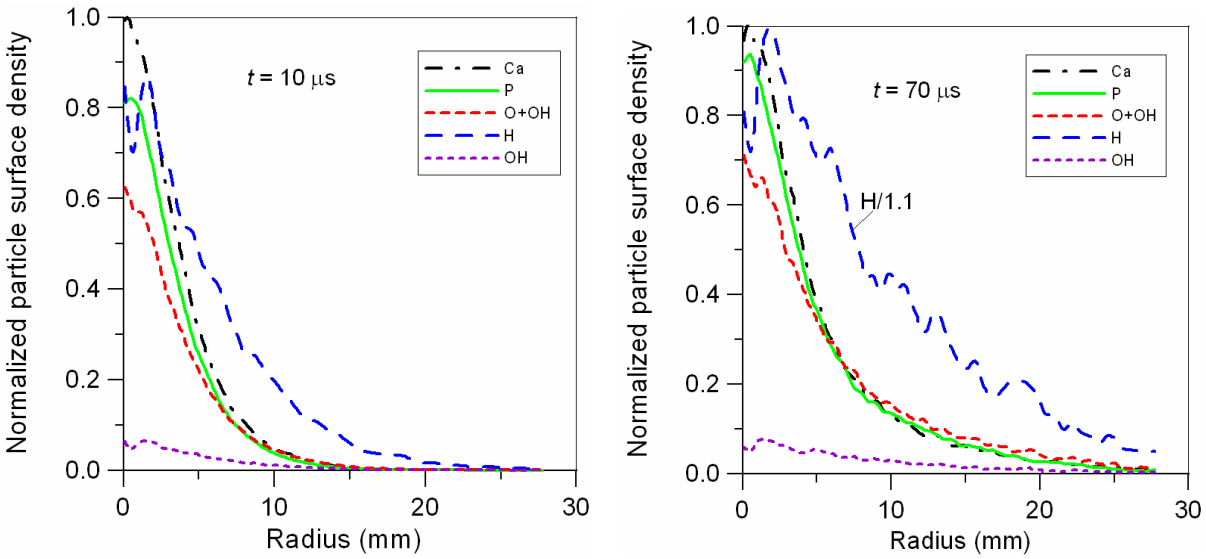

Fig.9. Normalized number of deposited particles per unit area as a function of radial distance from the centre of the substrate after 10 and 70 μs. Expansion into water vapour at a pressure of 20 Pa. Oxygen from OH radical is included in the oxygen density.

Fig. 9 presents spatial distributions of the number of particles per unit area deposited on the substrate as a function of a radial distance from the centre of the substrate at time t = 10 and 70 μs.

As expected in the case of heavier particles (see Fig.7) differences between the distributions of deposited particles after 10 and 70 μs are not large. Hydrogen is in excess all over the substrate area. After 70 μs the ratio of O:Ca (including oxygen from OH radical) and P:Ca is too low for the radii lower than 5 mm. The amount of hydrogen exceeds the amount necessary for the hydroxyapatite formation throughout the substrate.

The results indicate that also during the ablation in water vapour the stoichiometry of the HA target is not fully preserved, although it is much better than in the case of the ablation in vacuum. Better stoichiometry is achieved thanks to the particles supplied in the dissociation process which compensate the back- and sidescattering effects. Nevertheless crystalline films have been obtained [9-13] under similar experimental conditions.

4. Summary

The results show that stoichiometry can be seriously affected in the case of disparate masses of ablated particles. The ambient gas worsens the stoichiometry unless it supplies particles which compensate the backward and sideward flows of plume constituents. The ambient gas changes both the deposition rate and the angular distribution of deposited particles. Its presence results also in the transition from the rapid vacuum-like expansion to the diffusion-like regime.

The calculations give an insight into the stoichiometry of films deposited during the ablation of the hydroxyapatite target into vacuum and into the ambient water vapour. It has been shown that the stoichiometry cannot be preserved when ablating hydroxyapatite in vacuum and that the lack of hydrogen is mainly responsible for it. It is well known fact that in the case of the deposition in vacuum good HA coatings can be obtained after a post-deposition annealing in air [30,31]. It is conceivable that a post-deposition annealing in air, which always contains water vapour, restores the HA stoichiometry.

The stoichiometry of deposited films is significantly different when the ablation is carried out in ambient water vapour. The stoichiometry of deposited films is much

better although hydrogen reaches the substrate area in excess. However, the calculations indicate that the stoichiometry of the HA target is not fully preserved. On the other hand stoichiometric films of hydroxyapatite have been obtained experimentally under similar conditions. This means that the presented model is not complete and the additional parameters, in particular sticking coefficients, are necessary for a more reliable modelling of the deposition process.

References

1. H.M.Urbassek, D.Sibold D, Phys.Rev.Lett. **70,** 1886 (1993)
2. T.E.Itina, W.Marine, M.Autric, J.Appl.Phys. **82,** 3536 (1997)
3. E.Garrelie, C.Champeau, A.Catherinot, Appl.Phys.A **69,** 45 (1999)
4. T.E.Itina, J.Hermann, P.Delaporte, M.Sentis, Phys.Rev.E **66,** 066406 (2002)
5. T.E.Itina, J.Hermann, P.Delaporte, M.Sentis, Appl.Surf.Sc.**208**-**209,** 27 (2003)
6. A.N.Volkov, G.M.O'Connor, T.J.Glynn, G.A.Lukyanov, Appl.Phys.A **92,** 927 (2008)
7. A.A.Morozov, Zs.Geretovszky and T.Szörényi, J.Phys.D:Appl.Phys **41,** 015303 (2008)
8. J.Schou, Appl.Surf. Sci. **255,** 5191 (2009)
9. H.Zeng, W.R.Lacefield, S.Mirov, Biomed. Mater. Res.**50,** 248 (2000)
10. E.L.Solla, J.P.Borrajo, P.Gonzalez, J.Serra, S.Liste, S.Chiussi, B.Leon, B.Perez-Amor,, Appl. Surf. Sci. **248,** 360 (2005)
11. H.Kim, R.P.Camata, S.Lee, G.D.Rohrer, A.D.Rollett, Y.K.Vohra, Acta Materialia **55,** 131 (2007)
12. C.F.Koch, S.Johnson, D.Kumar, M.Jelinek, D.B.Chrisey, A.Doraiswamy, C.Jin, R.J.Narayan, I.N.Mihailescu, Mater.Sci.Eng.C **27,** 484 (2007)
13. V.Nelea, I.M.Mihailescu,M. Jelinek in *Pulsed Laser Application of Thin Films* edited by R. Eason (Wiley, Hoboken, 2007)
14. T.Ytrehus in *Rarefied Gas Dynamics* edited by J.L.Potter (Academic, New York, 1977)
15. C.J.Knight, AIAA Journal **17,** 519 (1979)
16. M.Jedynski, J.Hoffman, W.Mroz, Z.Szymanski, Appl.Surf.Sci. **255,** 2230 (2008)

17. J.L Arias, M.B.Mayor, J.Pou, B.Leon, M.Perez-Amor, Appl.Surf.Sci. **208**-**209,** 57 (2003)
18. G.A.Bird G A, *Molecular Gas Dynamics and the Direct Simulation of Gas Flows* (Clarendon, Oxford, 1994)
19. M.P.Allen, D.J.Tildesley, *Computer Simulation of Liquids* (Clarendon, Oxford, 2002)
20. http://www.americanelements.com
21. S. Yoo and X. C. Zeng, J.Chem Phys.**119,** 9518 (2002)
22. A.B.Murphy, C.J.Arundell, Plasma Chem. Plasma Process. **14,** 451 (1994)
23. J.R.Stallcop, E.Levin, H.Partridge, J.Thermophys. Heat Transfer **12,** 514 (1998)
24. J.R.Crifo, Astron.Astrophys.**223,** 365 (1989)
25. O.M. Belotserkovskii and V.E.Yanitskii, *Zh. Vychisl. Mat. Mat. Fiz*.(in Russian) **15,** 1553 (1975)
26. P.Maksyutenko, T.R.Rizzo, O.V.Boyarkin, J.Chem.Phys **125,** 181101 (2006)
27. P. Serra, J.L. Morenza, Appl. Surf. Sci. **127**–**129,** 662 (1998)
28. S. I. Anisimov, D. Bäuerle, and B. S. Luk'yanchuk, Phys. Rev.B **48**, 12 076 (1993).
29. S. Amoruso, B. Toftmann, J.Schou, Applied Surface Science **248,** 323 (2005)
30. V.Nelea, C.Ristoscu, C. Chiritescu, C.Ghica, I.M.Mihailescu, H.Pelletier., P.Mille, A.Cornet., Appl. Surf. Sci., **168,** 127 (2000)
31. M. Jedynski, J. Hoffman, T. Moscicki, W. Mroz, S. Burdynska, R. Ddiduszko, P. Kolodziejczak, Z. Szymanski, Materials Science-Poland **28**, 693 (2010)
32. P. Serra, J.M. Fernandez-Pradas, J. Navarro, J.L. Morenza, Appl. Phys. A **69**, S183 (1999)
33. P. Serra, J.L. Morenza, Appl. Phys. A **67**, 289 (1998)
34. L.I. Sedov, *Similarity and Dimensional Methods in Mechanics* (Mir Publishers, Moscow, 1982)
35. Ya.B. Zeldovich and Yu.P. Raizer, *Physics of Shock Waves and High-Temperature Hydrodynamic Phenomena* (Academic, NewYork, 1966)